

and magmatism in some areas (14, 45). In detail, the heterogeneous nature of the lithosphere probably contributes to the observed complexity in volcanic and tectonic patterns.

REFERENCES AND NOTES

- D. McKenzie and M. J. Bickle, *J. Petrol.* **25**, 713 (1988).
- D. M. Latin, J. E. Dixon, J. G. Fitton, N. White, in *Tectonic Events Responsible for Britain's Oil and Gas Reserves*, R. F. P. Hardman and J. Brooks, Eds. (Spec. Publ. 55, Geological Society of London, London, 1990), pp. 207–227.
- T. Pedersen and H. E. Ro, *Earth Planet. Sci. Lett.* **113**, 15 (1992).
- R. L. Armstrong and P. Ward, *J. Geophys. Res.* **96**, 13201 (1991); W. S. Snyder, W. R. Dickenson, M. L. Silberman, *Earth Planet. Sci. Lett.* **32**, 981 (1976).
- W. B. Hamilton, in *Metamorphism and Crustal Evolution of the Western United States*, W. G. Ernst, Ed. (Prentice-Hall, Englewood Cliffs, NJ, 1988), pp. 1–40.
- D. M. Miller, T. H. Nilsen, W. L. Bilodeau, in *The Cordilleran Orogen: Conterminous U.S.*, vol. G3, *The Geology of North America*, B. C. Burchfiel, P. W. Lipman, M. L. Zoback, Eds. (Geological Society of America, Boulder, CO, 1992), pp. 205–260.
- B. P. Wernicke, G. J. Axen, J. K. Snow, *Geol. Soc. Am. Bull.* **100**, 1738 (1988).
- N. L. Bogen and R. A. Schwieckert, *Earth Planet. Sci. Lett.* **75**, 93 (1985).
- R. E. Wells and P. L. Heller, *Geol. Soc. Am. Bull.* **100**, 325 (1988).
- N. Beghou and M. Barazangi, *Nature* **348**, 536 (1990).
- M. K. Savage, P. G. Silver, R. P. Meyer, *Geophys. Res. Lett.* **17**, 21 (1990).
- This statement excludes voluminous late Cenozoic hotspot-related magmatism of the Columbia River Plateau and Snake River Plain provinces that border the Great Basin to the north (17).
- P. B. Gans, G. A. Mahood, E. Schermer, *Geol. Soc. Am. Spec. Pap.* **233** (1989).
- M. G. Best and E. H. Christiansen, *J. Geophys. Res.* **96**, 13509 (1991).
- T. C. Feeley and A. L. Grunder, *Contrib. Mineral. Petrol.* **106**, 154 (1991).
- G. L. Farmer, D. E. Broxton, R. G. Warren, W. Pickthorn, *ibid.* **109**, 53 (1991).
- R. W. Carlson and W. K. Hart, *J. Geophys. Res.* **92**, 6121 (1987).
- R. L. Smith and R. G. Luedke, in *Explosive Volcanism: Inception, Evolution, and Hazards*, Geophysics Study Committee, Ed. (National Academy Press, Washington, DC, 1984), pp. 47–66.
- The later alkalic basalts closely resemble many oceanic island basalts in their trace element and isotopic characteristics, whereas compositions of the older tholeiitic basalts suggest they may be derived from distinct mantle sources, presumably within the lithosphere [J. G. Fitton, D. James, W. P. Leeman, *J. Geophys. Res.* **96**, 13593 (1991)]. This transition is diachronous in that true alkalic basalts erupted in the southern Great Basin only since ~5 Ma (38, 41, 42). In central Nevada they are uncommon and younger than 1 to 2 Ma [(39); C. C. Lum, thesis, Rice University, Houston (1992)]; none have been recognized in northern Nevada, Oregon, or Idaho. Although effects of crustal contamination cannot always be discounted, this pattern of compositional evolution suggests a change with time from initially lithospheric to asthenospheric sources in regions where alkalic basalts are present.
- M. A. Menzies, P. R. Kyle, M. Jones, G. Ingram, *J. Geophys. Res.* **96**, 13645 (1991).
- A. Nicolas, *J. Petrol.* **27**, 999 (1986).
- _____ and M. Jackson, *ibid.* **23**, 568 (1982).
- H. G. Wilshire, J. E. N. Pike, C. E. Meyer, E. L. Schwarzman, *Am. J. Sci.* **280-A**, 576 (1980); H. G. Wilshire *et al.*, *U.S. Geol. Surv. Prof. Pap.* **1443** (1988).
- D. L. Turcotte, *Annu. Rev. Earth Planet. Sci.* **10**, 397 (1982).
- B. S. Singer, J. D. Myers, S. R. Linneman, C. L. Angevine, *J. Volcanol. Geothermal Res.* **37**, 273 (1989).
- J. K. Meen, *Geol. Soc. Am. Spec. Pap.* **215** (1987), pp. 91–100.
- M. Wilson and H. Downes, *J. Petrol.* **32**, 811 (1991).
- D. McKenzie, *Earth Planet. Sci. Lett.* **40**, 25 (1978).
- Eq. 1 implies that volume is conserved during extension (28). In this model, the rate of lithospheric thinning decreases with time. An important consequence is that conductive cooling of the lower lithosphere is more pronounced at high degrees of extension, when the rate of lithospheric thinning is low.
- D. L. Harry, D. Sawyer, W. P. Leeman, *Earth Planet. Sci. Lett.* **117**, 59 (1993).
- M. Liu and C. G. Chase, *ibid.* **104**, 151 (1991).
- L. J. Sonder, P. C. England, B. P. Wernicke, R. L. Christiansen, in *Continental Extensional Tectonics*, M. P. Coward, J. F. Dewey, P. L. Hancock, Eds. (Spec. Publ. 28, Geological Society of London, London, 1987), pp. 187–201.
- Lamproitic magmas emplaced during the Eocene in the northern Rocky Mountains [F. O. Dudas, *J. Geophys. Res.* **96**, 13261 (1991); H. E. O'Brien, A. J. Irving, I. S. McCallum, *ibid.*, p. 13237] might be produced by such a process, but they are small in volume and compositionally dissimilar to volcanic rocks associated with mid-Tertiary extension (15, 17, 40).
- R. N. Thompson, *Contrib. Mineral. Petrol.* **52**, 213 (1975).
- J. R. Lister, *Earth Planet. Sci. Lett.* **107**, 233 (1991).
- P. B. Gans, *Tectonics* **6**, 1 (1987).
- Thompson's experiments (34) describe the solidus to liquidus phase relations in a typical olivine tholeiite from the Snake River Plain to pressures of 35 kbar. With his analyses of P_2O_5 content in the experimental glasses, and assuming that phosphorus is not included in any solid phase, we calculated the fraction (F) of glass (melt) for each analyzed experiment. The extent of melting was determined as a function of excess temperature above the solidus ($T_{\text{excess}} = [T_{\text{experiment}} - T_{\text{solidus}}]/[T_{\text{liquidus}} - T_{\text{solidus}}]$) at the respective pressure of each experiment. The variables T_{excess} and F are linearly correlated, and their relation is expressed as $F = 0.1703 + 0.7342 T_{\text{excess}}$. The non-zero intercept is partly an artifact of the difficulties of detecting and analyzing small amounts of glass in runs used to define solidus temperatures.
- D. S. Ormerod, C. J. Hawkesworth, N. W. Rogers, W. P. Leeman, M. A. Menzies, *Nature* **333**, 349 (1988).
- C. C. Lum, W. P. Leeman, K. A. Foland, J. A. Kargel, J. G. Fitton, *J. Geophys. Res.* **94**, 7871 (1989).
- J. G. Fitton, D. James, W. P. Leeman, *ibid.* **96**, 13693 (1991); K. J. Fraser, C. J. Hawkesworth, A. J. Erlank, R. H. Mitchell, B. H. Scott-Smith, *Earth Planet. Sci. Lett.* **76**, 57 (1985).
- E. E. Daley and D. J. DePaolo, *Geology* **20**, 104 (1992).
- T. K. Bradshaw, C. J. Hawkesworth, K. Gallagher, *Earth Planet. Sci. Lett.* **116**, 45 (1993).
- R. L. Christiansen and P. W. Lipman, *Philos. Trans. R. Soc. London Ser. A* **271**, 249 (1972).
- W. P. Leeman and J. G. Fitton, *J. Geophys. Res.* **94**, 7682 (1989).
- G. J. Axen, W. J. Taylor, J. M. Bartley, *Geol. Soc. Am. Bull.* **105**, 56 (1993).
- T. J. Falloon and D. H. Green, *Earth Planet. Sci. Lett.* **94**, 364 (1989).
- B. Parsons and D. McKenzie, *J. Geophys. Res.* **83**, 4485 (1978).
- We thank J. Oldow and D. Sawyer for discussions about the modeling. Partially supported by NSF grant EAR90-18437 (W.P.L.).

19 July 1993; accepted 30 September 1993

High- T_C Molecular-Based Magnets: Ferrimagnetic Mixed-Valence Chromium(III)-Chromium(II) Cyanides with T_C at 240 and 190 Kelvin

T. Mallah, S. Thiébaud, M. Verdaguer,* P. Veillet

Molecular-based magnets with high magnetic-ordering temperatures, T_C , can be obtained by mild chemistry methods by focusing on the bimetallic and mixed-valence transition metal μ -cyanide of the Prussian blue family. A simple orbital model was used to predict the electronic structure of the metal ions required to achieve a high ordering temperature. The synthesis and magnetic properties of two compounds, $[\text{Cr}_6(\text{CN})_{12}] \cdot 10\text{H}_2\text{O}$ and $\text{Cs}_{0.75}[\text{Cr}_{2.125}(\text{CN})_6] \cdot 5\text{H}_2\text{O}$, which exhibited magnetic-ordering temperatures of 240 and 190 kelvin, respectively, are reported, together with the strategy for further work.

The synthesis of well-characterized molecular-based magnets with Curie temperatures, T_C 's, close to room temperature remains a challenge (1–4). We are trying to prepare molecular-based materials of low

density that are transparent and have a tunable high T_C .

For our work, the classical cyanide system, based on Prussian blue (5, 6), is particularly useful because (i) the synthesis of bimetallic or mixed-valence systems is easy and flexible, relying on the reaction of stable hexacyanometallates {octahedral $[\text{B}(\text{CN})_6]^{k-}$ Lewis bases, which can be used as molecular building blocks} with metallic cations $\text{A}^{\ell+}$ (Lewis acids, used as assembling entities), where A and B can be transition metal ions with various oxidation

T. Mallah, S. Thiébaud, M. Verdaguer, Laboratoire de Chimie des Métaux de Transition, U.A. Centre National de la Recherche Scientifique 419, Université Pierre et Marie Curie, 4 Place Jussieu, 75252 Paris, France. P. Veillet, Institut d'Electronique Fondamentale, U.A. Centre National de la Recherche Scientifique 22, Université de Paris Sud, 91405 Orsay, France.

*To whom correspondence should be addressed.

and spin states; the starting molecular unit $[B(CN)_6]$ remains unchanged in the three-dimensional (3D) solid, hence our name of molecular-based materials; (ii) the structure of the resulting 3D network is highly symmetrical, most often a face-centered-cubic (fcc) frame of $[B(CN)_6]$ units connected by the metallic cations A in octahedral sites (7, 8); the general stoichiometric formula, $A_k[B(CN)_6]_l \cdot nH_2O$ can be modified by insertion of cations in the tetrahedral sites (Fig. 1) (9); and (iii) the nature and strength of the coupling constant J between the nearest neighbor ions A (spin S_A) and B (spin S_B) (with use of the interaction spin Hamiltonian $\mathbf{H} = -J \mathbf{S}_A \cdot \mathbf{S}_B$) can be analyzed within the binuclear fragment, $(NC)_5B-CN-A(NC)_5$, where B, C, N, and A are on a straight line.

The magnetic properties of such a system have already attracted much interest (3, 10, 11). Prussian blue itself, $Fe_4^{III}[Fe^{II}(CN)_6]_3 \cdot 15H_2O$, is a ferromagnet at low temperatures with $T_C = 5.5$ K (12). However, the Fe^{II} ions are low-spin (LS) d^6 [$S_{Fe^{II}}(LS) = 0$], and the interaction between the next-nearest neighbors Fe^{III} [high-spin (HS) d^5 , $S_{Fe^{III}}(HS) = 5/2$], more than 10 Å distant, is weak. A higher T_C implies two magnetic neighbors A and B with a stronger interaction J between them because $T_C \propto |J|$ (13, 14).

In our experiments, we used as the Lewis base the hexacyanochromate(III) ion, $[Cr^{III}(CN)_6]^{3-}$ [$B = Cr^{III}$, d^3 , $(t_{2g})^3$, $S_{Cr^{III}} = 3/2$]. Here, the three unpaired electrons are described by t_{2g} orbitals, delocalized on the cyanide ions, particularly on the nitrogen atoms (15, 16). These π -symmetry "magnetic orbitals" allow interactions in the three spatial directions. The choice of the A^{II} Lewis acid best-suited to combine with $[Cr^{III}(CN)_6]^{3-}$ and to obtain the desired

magnetic properties does not a priori demand a thorough mathematical treatment (17–21). There are two kinds of interactions between the t_{2g} magnetic orbitals of Cr^{III} and the singly occupied (magnetic) orbitals of the nearest neighbor A^{II} (when both A and B are octahedral). Neglecting the interaction between next-nearest neighbors, we observe that (case 1) when all the A^{II} magnetic orbitals have e_g symmetry (σ symmetry), the e_g (A) and t_{2g} (Cr) orbitals are orthogonal, and overlap is zero (Fig. 2A). This situation leads to a ferromagnetic contribution $J_{ab}(F)$ for each $t_{2g}(Cr)-e_g(A)$ orbital pair and to an overall ferromagnetic interaction between A and B ($J = J_F > 0$) (17, 22). These results are observed in $Cs^I Ni^{II} [Cr^{III}(CN)_6]_2 \cdot 2H_2O$, where we find evidence of a ferromagnetic short-range interaction between Cr^{III} and Ni^{II} and a 3D ferromagnetic ordering at $T_C = 90$ K (23, 24). On the other hand (case 2), when all the A^{II} magnetic orbitals have t_{2g} symmetry (π symmetry), the $t_{2g}(A)$ and $t_{2g}(Cr)$ orbitals overlap, and their interaction gives rise to two molecular orbitals with a Δ energy gap (Fig. 2B). The stronger the overlap, the larger the Δ energy gap and the stronger the antiferromagnetic contribution $J_{ab}(AF)$ (25, 26). Addition of the orbital contributions J_{ab} leads to an overall antiferromagnetic interaction between A and B ($J < 0$).

The general case is the superimposition of cases 1 and 2: Both t_{2g} and e_g electrons are on A^{II} , and the coupling constant J is the sum of the ferromagnetic ($J_F > 0$) and antiferromagnetic ($J_{AF} < 0$) orbital contributions. In this case, the antiferromagnetic term is often the leading one. For example, for $A^{II} = Mn^{II}$ [high-spin d^5 , $(t_{2g})^3$, $(e_g)^2$, $S_{Mn} = 5/2$], Babel demonstrated in $Cs^I Mn^{II} [Cr^{III}(CN)_6]$ that the antiferromagnetic short-range interaction between Cr^{III} and Mn^{II} , bearing different spins, induces a 3D ferrimagnetic order at $T_C = 90$ K (3).

We used this ferrimagnetic approach to reach higher T_C by increasing the antiferromagnetic coupling J between Cr^{III} and A^{II} with a suitable choice of A^{II} . Two routes are possible: increase the antiferromagnetic contribution $|J_{AF}|$ or decrease the ferromagnetic one J_F . Chromium(II) is a good candidate for A^{II} because it can work in both ways: High-spin Cr^{II} has a d^4 , $(t_{2g})^3$, $(e_g)^1$ Jahn-Teller distorted electronic configuration ($S_{Cr^{II}} = 2$). On one hand, it is less bulky than Mn^{II} and gives a shorter $Cr^{III}-CN-A^{II}$ distance, hence a stronger overlap between Cr^{III} and A^{II} t_{2g} orbitals and enlarged $t_{2g}(Cr^{III})-t_{2g}(A^{II})$ antiferromagnetic contributions; on the other hand, Cr^{II} has only one e_g magnetic orbital, instead of the two orbitals in Mn^{II} , and the weaker number of $t_{2g}(Cr^{III})-e_g(A^{II})$ ferromagnetic interactions induces a weaker resultant ferromagnetic term J_F .

The reaction of $K_3[Cr^{III}(CN)_6]$ and $Cr^{II}Cl_2$ in a deaerated aqueous medium under inert atmosphere affords a light gray precipitate (27). The elemental analysis is consistent with the formula $Cr_5(CN)_{12} \cdot 10H_2O$ [$Cr_3^{II}Cr_2^{III}(CN)_{12} \cdot 10H_2O$ from charge analysis]. The powder x-ray diffraction pattern is consistent with a fcc structure (unit cell $a = 10.34$ Å). Infrared (IR) spectroscopy in the 2000 to 2200 cm^{-1} region shows an intense single band at 2194 cm^{-1} , assigned to $Cr^{III}-CN-Cr^{II}$ links (28), similar to that found in $A_3^{II}[Cr^{III}(CN)_6]_2$ bimetallic compounds (23). These IR data are a first indication that all the cyanide bridges are bound to Cr^{III} through the carbon. In the visible region, the electronic spectrum shows weak, badly resolved bands of the two independent chromium chromophores. No absorption is observed in the near IR, in accord with localized unpaired electrons. In the photoelectron spectrum, the 2p chromium peak consists of two symmetrical bands assigned to Cr^{II} and Cr^{III} ions, in a 3/2 ratio; the 1s carbon peak is unique, as in $K_3[Cr(CN)_6]$, which confirms the bonding of the cyanide to Cr^{III} by the carbon: $\cdots NC-Cr^{III}-CN-Cr^{II} \cdots$.

Thermogravimetric analysis from room temperature to 600°C, in an inert atmosphere, shows a three-step curve. The first step between room temperature and 50°C corresponds to the loss of about four water molecules per formula unit. The second step, up to 230°C, corresponds to the loss of the six coordinated water molecules (two per Cr^{II} ion). Above 230°C, decomposition begins. The water molecules take up the $Cr^{III}(CN)_6$ vacancies; on average, two water molecules are bound to Cr^{II} , and the others are zeolitic. The mean coordination of chromium is therefore $Cr^{III}C_6$ and

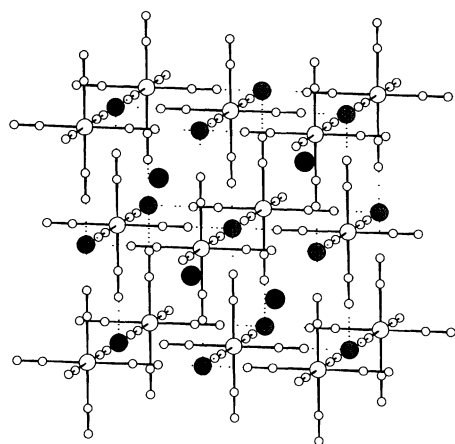


Fig. 1. Structure of the system $C^I A^{II} [B^{III}(CN)_6]$. Trivalent B^{III} , large white spheres; divalent A^{II} , large light gray spheres (octahedral sites); monovalent C^I , black spheres (tetrahedral sites); and carbon (bonded to B^{III}) and nitrogen (bonded to A^{II}), small white spheres.

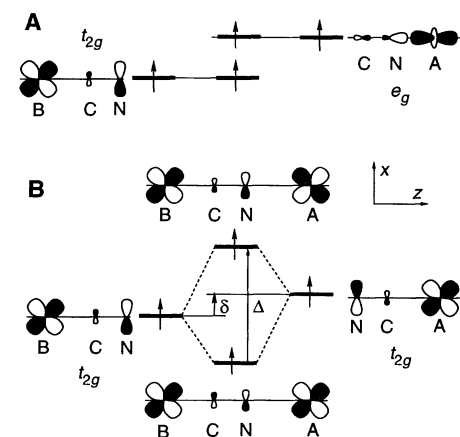


Fig. 2. Schematic orbital interaction in a $(NC)_5B-CN-A(NC)_5$ dinuclear unit. (A) Orthogonality between t_{2g} (xz) and e_g (z^2) magnetic orbitals ($B = Cr^{III}$; $A^{II} = Ni^{II}$). (B) Overlap between two t_{2g} (xz) magnetic orbitals [$B = Cr^{III}$; $A^{II} = any (t_{2g})^3$ ion]. For clarity, only the part of the orbitals located along the cyano bridge is shown.

$\text{Cr}^{\text{II}}\text{N}_4\text{O}_2$. The mean number of Cr^{II} neighbors of Cr^{III} is $z = 4$. The best formula is $\text{Cr}_3^{\text{III}}[\text{Cr}^{\text{III}}(\text{CN})_6]_2 \cdot 10\text{H}_2\text{O}$ (compound 1).

Faraday balance susceptibility measurements were carried out from $T = 390$ to 50 K. The product of the magnetic susceptibility and temperature, $\chi_M T$, first decreases continuously with temperature, from 390 K to a minimum at 290 K, and then climbs at lower temperatures (Fig. 3). Such behavior indicates a short-range antiferromagnetic interaction between nearest neighbor ions with different spins (ferrimagnetism). The linear part of the χ_M^{-1} versus temperature curve was fitted to the Curie-Weiss law $\chi_M = C_1/(T - \theta_1)$. The Curie constant is $C_1 = 8.1 \text{ cm}^3 \text{ mol}^{-1} \text{ K}$ [instead of the expected 12.75 (29)], and the Weiss constant $\theta_1 = -306$ K, indicating a large antiferromagnetic interaction between Cr^{III} and Cr^{II} through the cyanide bridge.

Magnetization measurements were performed with a superconducting quantum interference device (SQUID) magnetometer. The field-cooled magnetization versus temperature plot at $H = 5$ G shows a break at $T_C = 240$ K (Fig. 4, compound 1), which is the onset of 3D long-range ferrimagnetic order. Magnetization versus field measurements up to 7 T were carried out at $T = 10$ K (30). At $H = 7$ T, $M = 1.4$ Bohr magnetons, instead of the expected 6 (Fig. 5, compound 1), showing that the saturation is far from being complete. Finally, the magnetization versus field curve at 5 K, in the ± 100 G range, presents a hysteresis loop with a remnant magnetization $M_r = 1333 \text{ cm}^3 \text{ mol}^{-1} \text{ G}$ and a coercive field $H_c = 20$ G.

These results indicate that 1 is a 3D ferrimagnet with $T_C = 240$ K. Other magnetic measurements are necessary (at higher field, under pressure, and on single crystals when available) to better characterize the magnetization behavior, in particular to look for possible spin-canting.

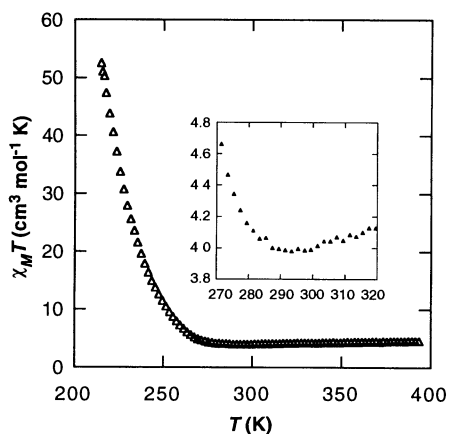


Fig. 3. Thermal variation of the susceptibility of compound 1, $\chi_M T$ versus T . (Insert) Expanded view of the minimum region.

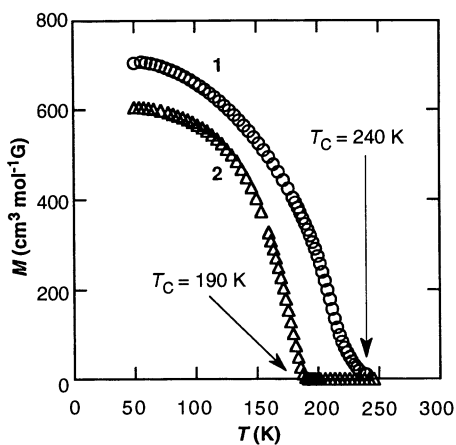


Fig. 4. Field-cooled magnetization versus temperature at $H = 5$ G for compound 1 (O) and compound 2 (Δ).

The value of T_C may be increased if z , the mean number of magnetic neighbors, is enhanced [$T_C \propto z$ (13)]. This is possible, in principle, by reduction of the $\text{Cr}(\text{CN})_6$ vacancies present in 1 (9) with the use of Cs^{I} salts during the synthesis, as previously demonstrated (3, 24). When $\text{Cs}_2\text{K}[\text{Cr}^{\text{III}}(\text{CN})_6]$, instead of $\text{K}_3[\text{Cr}^{\text{III}}(\text{CN})_6]$, was mixed with $\text{Cr}^{\text{II}}\text{Cl}_2$ in deaerated aqueous medium under inert atmosphere, a deep green precipitate (compound 2) was obtained. Reproducible elemental analysis of 2 is consistent with the formula $\text{Cs}_{0.75}[\text{Cr}_{2.125}(\text{CN})_6] \cdot 5\text{H}_2\text{O}$ [$\{\text{Cs}_{0.75}[\text{Cr}_{1.125}^{\text{II}}\text{Cr}_{1.00}^{\text{III}}(\text{CN})_6] \cdot 5\text{H}_2\text{O}$ from charge analysis} (31).

Compound 2 has a fcc structure (unit cell parameter $a = 10.38 \text{ \AA}$). The IR spectrum has two C-N stretching bands at 2069 and 2187 cm^{-1} . The 2069 cm^{-1} band suggests the presence of $\text{Cr}^{\text{II}}\text{-CN-Cr}^{\text{III}}$ links (32), in addition to those of $\text{Cr}^{\text{III}}\text{-CN-Cr}^{\text{II}}$, at 2187 cm^{-1} . In the photoelectron spectrum, the $2p$ chromium peak consists of two main bands, assigned to Cr^{III} and Cr^{II} ions. The $1s$ carbon peak

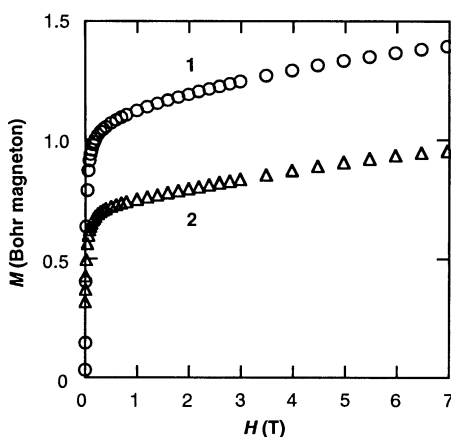


Fig. 5. First magnetization curve M versus H at $T = 10$ K for compound 1 (O) and compound 2 (Δ).

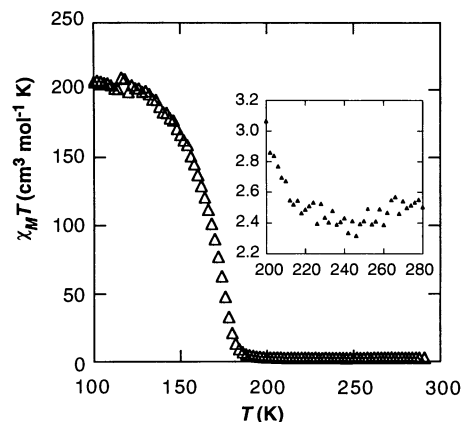


Fig. 6. Thermal variation of the susceptibility of compound 2, $\chi_M T$ versus T . (Insert) Expanded view of the minimum region.

displays two bands: one ($\approx 80\%$) can be assigned to carbon bound to Cr^{III} , $\text{Cr}^{\text{I}}\text{-}\mu\text{C}_6$, as in 1, and the other ($\approx 20\%$) to carbon bound to Cr^{II} . However, $\text{Cr}^{\text{II}}\text{C}_6$ corresponds to a low-spin state, $[(t_{2g})^4, S_{\text{Cr}^{\text{II}}}(\text{LS}) = 1]$. The amount of $\text{Cr}^{\text{II}}(\text{LS})$ is then $\leq 20\%$ of the total amount of Cr^{II} . The electronic spectrum shows a wide band centered at 1140 nm . The color can be assigned to some electron transfer between the two chromium ions (33).

The thermal variation of $\chi_M T$ for 2 (from Faraday balance measurements) is characteristic of ferrimagnetic behavior (Fig. 6). It is similar to that of 1, but the minimum occurs at 235 K. The high-temperature, linear part of the χ_M^{-1} versus temperature curve, fitted to the Curie-Weiss law $\chi_M = C_2/(T - \theta_2)$, yields a Curie constant $C_2 = 4.9 \text{ cm}^3 \text{ mol}^{-1} \text{ K}$ and a Weiss constant $\theta_2 = -440$ K. The θ_2 value indicates a large antiferromagnetic interaction between Cr^{III} and Cr^{II} . The Curie constant allows an independent estimate of the number of high-spin, N- and O-bonded Cr^{II} [$\text{Cr}^{\text{II}}(\text{HS}) = 0.95$] and of low-spin, C-bonded Cr^{II} [$\text{Cr}^{\text{II}}(\text{LS}) = 0.175$] (33), consistent with photoelectron spectroscopy. Compound 2 may then be formulated as $\{\text{Cs}_{0.75}[\text{Cr}_{0.95}^{\text{II}}(\text{HS}) \text{Cr}_{0.175}^{\text{III}}] [\text{Cr}_{0.825}^{\text{III}} \text{Cr}_{0.175}^{\text{II}}(\text{LS})] (\text{CN})_6\} \cdot 5\text{H}_2\text{O}$.

The field-cooled magnetization versus temperature plot at $H = 5$ G shows a break at $T_C = 190$ K (Fig. 4, compound 2), which is the onset of a 3D long-range ferrimagnetic order. The first magnetization versus field curve at $T = 10$ K (Fig. 5, compound 2) shows that magnetization at $H = 7$ T is close to that expected from antiferromagnetically coupled $\text{Cr}^{\text{III}}\text{-Cr}^{\text{II}}$ ions (0.95 Bohr magnetons instead of 1.125) (30).

Our results show that 2 behaves as a 3D ferrimagnet with $T_C = 190$ K. This T_C value is high. Nevertheless, it is lower than expected and even lower than the T_C in 1. There are two possible explanations for this

situation: (i) In our attempt to enhance ζ , the number of magnetic neighbors, we were only partially successful (in **2**, $\zeta = 16/3$, larger than $\zeta = 4$ in **1** but less than $\zeta = 6$ in the expected ideal structure); or (ii) the nonnegligible presence of low-spin Cr^{II} (0.175) in the B(CN)₆ sites induces a structural (and magnetic) disorder, which defeats our experimental strategy. The exchange interaction in **2** is therefore more complex than in **1**, and its detailed description would be beyond the scope of this note. It can be said, however, that the lowering of T_C in **2**, compared with **1**, is in large part a result of the fact that two t_{2g} unpaired electrons of the low-spin Cr^{II} present in **2** are less efficient in inducing antiferromagnetic interactions than the three of Cr^{III} in **1**.

An important property of the two compounds is their stability in atmospheric conditions: They may be left for weeks in the laboratory in bottles opened to air from time to time without apparent chemical change of Cr^{II} or loss of the magnetic properties. Such stability is surprising (the reduction properties of Cr^{II} are well-known) but valuable because it opens the possibility of useful applications at room atmosphere. The two compounds, stirred in hydrochloric acid (1 mol liter⁻¹) for 24 hours and then dried under vacuum at 100°C, remain unchanged on return to room atmosphere. In both compounds, the μ -cyano Cr^{III}-Cr^{III} insoluble network, as soon as it is formed, appears robust and chemically inert.

The deep green compound **2** deserves further comment: It displays in the near IR, in contrast to the light gray **1**, an intense absorption band centered at 8720 cm⁻¹, a much lower energy than that of the intervalence band of Prussian blue (15,000 cm⁻¹) (34). Hence, **2** presents a higher T_C (190 K compared with 5.5 K) and an easier electronic delocalization than Prussian blue. These two associated properties can open new perspectives in the field, and we consider **2** as the first member of a series of promising new systems.

We are now engaged in a more complete characterization of the two compounds and, in particular, in the study of their magneto-optical properties. Growth of single crystals and new syntheses are in progress in order to obtain new bimetallic and mixed-valence systems with higher T_C .

REFERENCES AND NOTES

1. O. Kahn, *Molecular Magnetic Materials*, D. Gatteschi, O. Kahn, J. S. Miller, F. Palacio, Eds. (NATO Advanced Study Institutes Series, Ser. E, Kluwer, Dordrecht, Netherlands 1991), vol. 198, pp. 35–52; J. S. Miller, *ibid.*, pp. 151–158; P. Rey, *ibid.*, pp. 203–214; A. Caneschi, *ibid.*, pp. 215–232; V. Gadet, *ibid.*, pp. 281–295.
2. J. M. Manriquez *et al.*, *Science* **252**, 1415 (1991).
3. W. D. Griebler and D. Babel, *Z. Naturforsch. Teil B* **87**, 832 (1982).
4. P.-M. Allemand *et al.*, *Science* **253**, 301 (1991).
5. M. Woodward, *Philos. Trans. R. Soc. London* **33**, 15 (1734).

6. B. N. Figgis and J. Lewis, in *Progress in Inorganic Chemistry*, F. A. Cotton, Ed. (Wiley-Interscience, New York, 1964), vol. 6, p. 188.
7. H. U. Gudel, H. Stucki, A. Lüdi, *Inorg. Chim. Acta* **7**, 121 (1973).
8. A. Lüdi and H. U. Gudel, in *Structure and Bonding* J. D. Dunitz *et al.*, Eds. (Springer-Verlag, Berlin, 1973), vol. 14, pp. 1–21.
9. The k/l ratio depends on the charges of A and B; when $k/l > 1$, B(CN)₆ vacancies occur and are filled by water molecules. For B^{III} and A^I, the formula is $A_2[B(CN)_6]_3 \cdot nH_2O$; $k/l = 3/2$, and 1/3 of the B(CN)₆ sites are vacant. A has a mean of $z = 4$ B neighbors. Insertion of Cs^I in half of the tetrahedral sites of the network suppresses the vacancies and leads to a 1/1 stoichiometry: $Cs[A^I B^III(CN)_6] \cdot nH_2O$, A now having $z = 6$ B neighbors.
10. A. N. Holden *et al.*, *Phys. Rev.* **102**, 1463 (1956).
11. R. M. Bozorth *et al.*, *ibid.* **103**, 572 (1956).
12. A. Ito, M. Suenaga, K. Ono, *J. Chem. Phys.* **48**, 3597 (1968).
13. The results of such an analysis in 3D ferrimagnets, done with mean field theory and neglect of direct interaction between next-nearest neighbors (14), lead to $T_C = z |J| \sqrt{(C_A C_B)}/N_A g^2 \mu_B^2$, where z is the number of nearest magnetic neighbors, C_A and C_B are Curie constants, g is the mean g factor for A and B, and μ_B is the Bohr magneton.
14. L. Néel, *Ann. Phys. Paris* **3**, 10 (1948).
15. The spin delocalization on the cyanide ion was experimentally demonstrated by spin-polarized neutron studies (16).
16. B. N. Figgis, J. B. Forsyth, P. A. Reynolds, *Inorg. Chem.* **26**, 101 (1989).
17. Such a treatment is available through various models of exchange interaction (18–21) that define differently the wave functions (a) and (b) describing the unpaired electrons 1 and 2 on centers A and B. Different but equivalent expressions of J are therefore available. It is convenient to consider J as the sum of the different orbital interactions (or exchange pathways) J_{ab} , themselves split into antiferromagnetic [$J_{ab}(AF) < 0$] and ferromagnetic [$J_{ab}(F) > 0$] terms

$$J \propto \sum_{a,b} J_{ab} \propto \sum_{a,b} J_{ab}(F) + J_{ab}(AF) = J(F) + J(AF)$$

In a model of localized electrons (21), $J_{ab}(F)$ is related to the bielectronic exchange integral $j = \langle a(1) b(2) | e^2/r_{12} | a(2) b(1) \rangle$: $J_{ab}(F) \propto j$ and $J_{ab}(AF)$ is related to the mono-electronic overlap integral $S = \langle a(1) | b(1) \rangle$: $J_{ab}(AF) \propto S^2$.

18. P. W. Anderson, in *Magnetism*, G. T. Rado and H. Suhl, Eds. (Academic Press, New York, 1963), vol. 1, p. 25.
19. J. B. Goodenough, *Magnetism and the Chemical Bond* (Wiley, New York, 1963).
20. P. J. Hay, J. C. Thiebault, R. Hoffmann, *J. Am. Chem. Soc.* **97**, 4884 (1975).
21. O. Kahn, in *Magneto-Structural Correlations, in Exchanged Coupled Systems*, D. Gatteschi, O. Kahn, R. D. Willett, Eds. (Reidel, Dordrecht, Netherlands, 1985), p. 37.
22. All the antiferromagnetic terms are zero and six t_{2g} - e_g ferromagnetic exchange pathways are present: $J \propto \sum_{eg, t2g} J_{ab}(F) = J_F > 0$.
23. V. Gadet, thesis, Université Pierre et Marie Curie, Paris (1992).
24. ———, T. Mallah, I. Castro, P. Veillet, M. Verdaguier, *J. Am. Chem. Soc.* **114**, 9213 (1992).
25. It has been proposed (21, 26) that when the energies of a and b orbitals are different, as in Figure 2B, $J_{ab}(AF) \propto S \sqrt{(\Delta^2 - \delta^2)}$, where Δ and δ are defined in Fig. 2B. Most often, when $S \neq 0$, $|J_{ab}(AF)| > J_{ab}(F)$.
26. P. Tola, O. Kahn, C. Chauvel, H. Coudanne, *Nouv. J. Chim.* **1**, 467 (1977).
27. The same compound, **1**, is obtained from the reaction of solutions of $K_4[Cr^{II}(CN)_6]$ with $Cr^{III}Cl_3$, under similar conditions. The unit cell formula of **1** is $\{Cr_4^{II} [Cr^{III}(CN)_6]_{8/3} []_{4/3} (H_2O)_{40/3}\}$, where [] stands for $[B(CN)_6]$ vacancies.
28. K. Nakamoto, *Infrared and Raman Spectra of Inorganic and Coordination Compounds* (Wiley, New York, ed. 3, 1978), pp. 259–267.
29. Assuming a mean $g = 2$ value for Cr^{III} and Cr^{II} ions and $N_A \mu_B^2/3k = 1/8$.
30. No appreciable change was observed during operation at $T = 2$ K.
31. Traces of potassium and chlorine (<0.3%) appear in some preparations, without significant change of the magnetic properties. The unit cell formula of **2** is $Cs_{8/3} [Cr_4^{II} Cr_{32/9}^{III} (CN)_{192/9} []_{4/9} (H_2O)_{160/9}]$, where [] stands for $[B(CN)_6]$ vacancies.
32. J. P. Eaton and D. Nicholls, *Transition Met. Chem.* **6**, 203 (1981).
33. We plan to check the assumption of an intervalence band by examining the electronic spectra at low temperature.
34. M. B. Robin, *Inorg. Chem.* **1**, 337 (1962).
35. We acknowledge I. Castro, M. Delamare, F. Hardouin, C. Hélay, Y. Journaux, C. Mathonnière, and F. Robert for their help in the experimental studies.

12 July 1993; accepted 20 September 1993

Binding to DNA and the Retinoblastoma Gene Product Promoted by Complex Formation of Different E2F Family Members

Wilhelm Krek, David M. Livingston,* Suman Shirodkar

The E2F family of transcription factors functions in the control of the mammalian cell cycle. Here it is shown that two family members, E2F-1 and DP-1, form specific heterodimers *in vivo*, a process that enhances DNA binding, transactivation, and the binding of the retinoblastoma gene product. These results suggest that heterodimerization regulates E2F function and contributes to cell cycle control.

The E2F family of transcription factors (1) contributes to cell cycle regulation through the controlled activation of certain growth-

responsive genes (2). Complementary DNAs (cDNAs) from two family members, E2F-1 and DP-1, were cloned and shown to be components of Rb-E2F complexes (3–6). Because E2F can bind its cognate DNA binding motif as a complex of different subunits *in vitro* (7), we examined whether

Dana-Farber Cancer Institute and Harvard Medical School, Boston, MA 02115.

*To whom correspondence should be addressed.